Please cite this article in press as: Real Hernandez and Levental, Lipid packing is disrupted in copolymeric nanodiscs compared with intact membranes, Biophysical Journal (2023), https://doi.org/10.1016/j.bpj.2023.01.013

Biophysical Journal
Article

Biophysical Society

Lipid packing is disrupted in copolymeric nanodiscs compared with intact membranes

Luis M. Real Hernandez[1] and Ilya Levental[1,*]
[1]Department of Molecular Physiology and Biological Physics, Center for Membrane and Cell Physiology, University of Virginia, Charlottesville, Virginia

ABSTRACT Discoidal lipid-protein nanoparticles known as nanodiscs are widely used tools in structural and membrane biology. Amphipathic, synthetic copolymers have recently become an attractive alternative to membrane scaffold proteins for the formation of nanodiscs. Such copolymers can directly intercalate into, and form nanodiscs from, intact membranes without detergents. Although these copolymer nanodiscs can extract native membrane lipids, it remains unclear whether native membrane properties are also retained. To determine the extent to which bilayer lipid packing is retained in nanodiscs, we measured the behavior of packing-sensitive fluorescent dyes in various nanodisc preparations compared with intact lipid bilayers. We analyzed styrene-maleic acid (SMA), diisobutylene-maleic acid (DIBMA), and polymethacrylate (PMA) as nanodisc scaffolds at various copolymer-to-lipid ratios and temperatures. Measurements of Laurdan spectral shifts revealed that dimyristoyl-phosphatidylcholine (DMPC) nanodiscs had increased lipid headgroup packing compared with large unilamellar vesicles (LUVs) above the lipid melting temperature for all three copolymers. Similar effects were observed for DMPC nanodiscs stabilized by membrane scaffolding protein MSP1E1. Increased lipid headgroup packing was also observed when comparing nanodiscs with intact membranes composed of binary mixtures of 1-palmitoyl-2-oleoyl-phosphocholine (POPC) and di-palmitoyl-phosphocholine (DPPC), which show fluid-gel-phase coexistence. Similarly, Laurdan reported increased headgroup packing in nanodiscs for biomimetic mixtures containing cholesterol, most notable for relatively disordered membranes. The magnitudes of these ordering effects were not identical for the various copolymers, with SMA being the most and DIBMA being the least perturbing. Finally, nanodiscs derived from mammalian cell membranes showed similarly increased lipid headgroup packing. We conclude that nanodiscs generally do not completely retain the physical properties of intact membranes.

SIGNIFICANCE Copolymeric nanodiscs have become popular for isolation of membrane proteins from their endogenous membrane environments. We investigated whether nanodiscs stabilized by various copolymers retain the lipid packing of intact membranes using Laurdan and analogous reporters. Lipid packing was compared between nanodiscs and intact bilayers using membranes of increasing lipid complexity from single component to biological membranes. More packed lipid headgroups were consistently observed in nanodiscs compared with intact bilayers, most evident for relatively fluid bilayers. We found that copolymeric nanodiscs generally do not retain lipid headgroup packing of unperturbed membranes. Our results highlight the need to carefully consider how membrane structure is perturbed when using nanodiscs as membrane models.

INTRODUCTION

Transmembrane proteins comprise ~30% of the mammalian proteome and carry out essential functions such as signal transduction and solute exchange (1,2). They also comprise a major fraction of the targets of pharmaceutical drugs (3). Although their importance in cellular function is well established, membrane proteins have historically been challenging to study due to difficulties inherent in stabilizing their hydrophobic transmembrane regions during isolation (4). Classical methods rely on detergents, which efficiently remove lipids and solvate hydrophobic transmembrane regions (5). Although these methods have been extensively used and are effective, there is a possibility of artifactual and unexpected effects of the detergents on protein structure and function (6). More significantly, membrane proteins in situ are solvated and regulated by their surrounding lipid matrix (7,8). Detergents remove most

Submitted August 31, 2022, and accepted for publication January 11, 2023.
*Correspondence: il2sy@virginia.edu
Editor: Siewert Jan Marrink.
https://doi.org/10.1016/j.bpj.2023.01.013

Please cite this article in press as: Real Hernandez and Levental, Lipid packing is disrupted in copolymeric nanodiscs compared with intact membranes, Biophysical Journal (2023), https://doi.org/10.1016/j.bpj.2023.01.013

such lipids, preventing analysis of lipids associated with membrane proteins and how they may regulate protein behavior.

Membrane lipids can regulate transmembrane protein structure and function in multiple ways (9). Lipids can directly bind to transmembrane proteins to allosterically modulate their activity, as has been suggested for cholesterol (10,11). Membrane biophysical properties can be modified by lipid compositions to regulate protein conformation and activation, as has been shown for the adenosine 2A receptor (12). Protein oligomerization is often influenced by both individual membrane lipids, as shown for phosphatidylinositol-4,5-bisphosphate (PIP2) (13,14), and membrane collective properties (15–17). By preserving the lipid environment surrounding transmembrane proteins, the mechanisms by which lipids influence protein conformation and function can be better understood.

One solution to recapitulating the lipid environment around proteins is to re-incorporate detergent-isolated proteins into synthetic proteoliposomes (18). Although this approach recovers some features of membrane lipid interactions, it requires extensive experimental measures to confirm protein orientation, is not easily adaptable between different proteins, and still requires the use (and associated caveats) of detergents (19–21). An alternative to proteoliposomes is incorporation of transmembrane proteins from detergent micelles into nanodiscs. Nanodiscs are discoidal lipid bilayer nanoparticles stabilized by a polymeric, amphipathic scaffold that encircles the lipid bilayer (22). The most commonly used scaffolds are membrane scaffold proteins (MSPs) (23), which are engineered from the amphipathic α-helices of apolipoprotein A (23,24). MSP nanodiscs are formed via similar approaches to proteoliposomes; i.e., removing detergent molecules in the presence of bilayer-forming lipids (25). MSP-scaffolded nanodiscs have gained popularity in recent years because of their effectiveness in solubilizing membrane proteins with a skirt of bilayer lipids for structural characterization by cryoelectron microscopy (26).

Although MSP nanodiscs require detergent solubilization of proteins before nanodisc incorporation, transmembrane proteins with surrounding lipid shells can instead be directly extracted from membranes by synthetic, amphipathic copolymers (27). The term nanodisc was originally coined for discoidal lipid nanoparticles stabilized by MSPs, but various synthetic copolymers can also form similar particles, with a peripheral copolymer scaffold stabilizing a lipid core (28). In this work, we use the term nanodisc to describe all discoidal lipid bilayer nanoparticles, regardless of scaffold. Copolymeric nanodiscs have the advantage of solubilizing membrane proteins without detergents (29), because they directly intercalate into membranes and eventually dissolve them after sufficient copolymer incorporation (30). Schematic models of copolymeric nanodisc formation often imply a "cookie-cutter" mechanism, in which copolymers surround a nanoscopic patch of membrane and extract it from the membrane; however, molecular dynamic simulations do not support such a mechanism (31). Rather, it seems that copolymers, such as the widely used styrene-maleic acid (SMA), bind to, intercalate into, and eventually solubilize membranes via complex and poorly detailed pathways, which may alter the properties of the target membranes (32,33).

Because copolymeric nanodiscs are directly isolated from membranes without detergents (34,35), a tempting hypothesis is that they isolate the native membrane regions around transmembrane proteins. Copolymeric nanodiscs do isolate and solubilize native membrane lipids (36); however, various copolymers preferentially solubilize certain membrane proteins and lipids, with membrane biophysical properties being suggested as a driving factor for these preferences (37). As such, it remains unclear how well copolymeric nanodiscs retain the collective properties of the membrane from which they are extracted (throughout this work, native/unperturbed/intact membrane refers to the bilayers from which nanodiscs are formed, regardless of composition). Here, we evaluate whether lipid headgroup packing is retained in copolymeric nanodiscs using the extensively characterized solvatochromic fluorescent reporterLaurdan and its analogs to compare lipid vesicles with nanodiscs of the same composition (38). In general, we find that Laurdan consistently reports less hydrated, more tightly packed lipid headgroups in nanodiscs relative to unperturbed bilayers across various lipid compositions, temperatures, and copolymer chemistries. As a complementary method, lateral membrane pressure was measured using Flipper-TR, showing that some nanodisc preparations had decreased lateral membrane pressure compared with unperturbed membranes. We conclude that nanodiscs do not generally retain the physical properties of intact membranes, although there are notable differences between various copolymers, suggesting that 1) careful choices of experimental conditions may mitigate some of the effects, and 2) continued development of copolymers may produce nanodisc formulations that better maintain native membrane properties.

MATERIALS AND METHODS

Materials

1,2-Dimyristoyl-sn-glycero-3-phosphocholine (DMPC), 1-palmitoyl-2-oleoyl-glycero-3-phosphocholine (POPC), 1,2-dipalmitoyl-sn-glycero-3-phosphocholine (DPPC), N-palmitoyl-D-erythro-sphingosylphosphoryl (PSM), cholesterol (CH), Laurdan, and polymethacrylate N−C4−52−6.9 (PMA) copolymer (880134) were purchased from Avanti Polar Lipids (Alabaster, AL). EGTA was purchased from Sigma-Aldrich (St Louis, MO). C-Laurdan was purchased from SFC (Chunbuk, Republic of Korea). Pro12A was obtained as a gift from Andrey Klymchenko (39). SMA (SMALP 200) and diisobutylene-maleic acid (DIBMA; DIBMA 12) copolymers buffered with HEPES were purchased as powders from Cube Biotech (Monhein, Germany). Flipper-TR was purchased from Cytoskeleton (Denver, CO). All other reagents were purchased from Thermo Fisher Scientific (Waltham, MA) unless stated otherwise.

Please cite this article in press as: Real Hernandez and Levental, Lipid packing is disrupted in copolymeric nanodiscs compared with intact membranes, Biophysical Journal (2023), https://doi.org/10.1016/j.bpj.2023.01.013

Large unilamellar vesicle preparation

Lipid solutions were added to amber glass vials using glass syringes at room temperature (22°C). These solutions were dried under a gentle stream of N_2 and then vacuum desiccated overnight to remove residual solvent. Lipid films were hydrated with HEPES buffer (20 mM HEPES, 150 mM NaCl, 2 mM EDTA, 2 mM EGTA, pH 7.4) at 37°C for 1 h with vortexing every 15 min. The resulting multilamellar lipid suspensions were subjected to five freeze-thaw cycles. All suspensions were frozen at the same temperature (−70°C). DMPC suspensions were thawed at 40°C, whereas all other suspensions were thawed at 60°C. Temperatures were chosen such that the thawing temperature was above the melting point of all phospholipids in the mixture. After freeze-thawing, suspensions were extruded 31 times through polycarbonate membranes with a nominal pore size of 100 nm (Whatman). DMPC samples were extruded at 40°C, whereas all other samples were extruded at 60°C. Resulting large unilamellar vesicles (LUVs) were stored at room temperature (22°C) until use.

HEK293 crude membrane collection

HEK293 cells were cultured in Eagle's minimal essential media (EMEM) containing sodium bicarbonate (1.5 g/L), L-glutamine (292 mg/L), sodium pyruvate (110 mg/L), and non-essential amino acids supplemented with 10% fetal calf serum (FCS) at 37°C in humidified 5% (v/v) CO_2 air. HEK293 cells were grown in 100-mm dishes to 90% confluency, washed with ice-cold PBS (10 mM, pH = 7.4), and then scraped over ice into 3 mL/dish of HEPES buffer (20 mM HEPES, 150 mM NaCl, 2 mM EDTA, 2 mM EGTA, 1× Halt protease inhibitor cocktail, pH 7.4). Collected samples were probe sonicated three times for 10 s at an amplitude ∼70 μm (model Q55 with probe 4422, Qsonica Sonicators) with 30-s intermediate incubations on ice between sonications. Resulting lysates were centrifuged at 100,000 × g for 1 h at 4°C to collect crude membrane pellets. The wet mass of each pellet was determined, and the pellets were resuspended with HEPES buffer used for cell collection to a concentration of 40 mg crude membrane per milliliter. Crude membrane samples were stored at 4°C until further use.

Nanodisc formation

The copolymers SMA, DIBMA, and PMA were used to form nanodiscs (Fig. 1 *A*). Copolymer powders were hydrated as received with HEPES buffer (20 mM HEPES, 150 mM NaCl, 2 mM EDTA, 2 mM EGTA, pH 7.4) to make 0.1 g/mL stock solutions. Copolymer weight average molar masses were SMA = 6500 g/mol, DIBMA = 12,000 g/mol, and PMA = 6900 g/mol. To ensure nanodisc formation, a set of samples were formed above the copolymer-to-lipid ratio (R_{SOL}) known to fully solubilize bilayers into nanodiscs. R_{SOL} values are dependent on both the copolymer and lipids, and can be measured by analyzing the intensity of 31P NMR signals upon titration of copolymer into LUV suspensions (30). These intensities can be fit to a detergent solubilization model, where the copolymer solubilization concentration is defined as the concentration at which NMR signal intensity no longer increases (i.e., all membranes are solubilized). R_{SOL} is then determined by a linear fit to the relationship between this copolymer solubilization concentration and the concentration of lipid for a range of lipid concentrations. Copolymers were mixed with LUVs to a desired copolymer-to-lipid ratio, and then diluted with HEPES buffer to a final total lipid concentration of 0.2 mM. LUV samples with copolymer were then incubated for 1 h at 40°C for DMPC samples and 60°C for all other samples. These temperatures were used to ensure that all phospholipids in the samples were in a fluid phase during solubilization, to avoid lipid phase solubility preferences by the copolymers. After incubation, the samples were analyzed without further purification. MSP1E1 DMPC nanodiscs were a kind gift of the Reichow lab and prepared as previously published (40).

For generating copolymeric nanodiscs from HEK293 membranes, crude membrane samples were diluted to a concentration of 10 mg/mL in the presence of 1 mg of SMA or DIBMA per gram of wet membrane mass. This concentration of copolymer has been reported to be sufficient to solubilize *Escherichia coli* membranes (42). We used the minimal possible concentrations of copolymers required to solubilize most cell membranes to avoid introducing artifacts from excess copolymer (43). Samples were then incubated at 37°C for 1 h, including control samples without added copolymer. Undissolved material was removed by centrifugation at 18,000 × g for 1 h at 4°C, and collected supernatants containing nanodiscs were transferred into amber glass vials. Supernatants were diluted five-fold before analysis, and stored at 4°C.

Dynamic light scattering

Dynamic light scattering (DLS) measurements were performed using a Zetasizer Nano ZS90 (Malvern Instruments, Worcestershire, UK) equipped with a 633-nm He-Ne laser and a 90° detector. Copolymer was incubated with samples containing 6 mM DMPC for 1 h at 40°C. Samples were analyzed at 30°C in disposable polycyclic olefin microcuvettes (BrandTech Scientific, Essex, CT). Experimental parameters were set using TetraSpeck microspheres (d = 100 nm). All samples were measured three times, with attenuator position automatically optimized for each measurement. Data analysis was performed using instrument software, with intensity-weighted particle size distribution determined using a non-negatively constrained least-squares function and z-average particle size and polydispersity index (PDI) determined by cumulant analysis.

Fluorescent dye staining

Laurdan was added from methanol stock to lipid-only samples (those not derived from biological membranes) at a molar ratio of 200:1 lipid to Laurdan before lipid film formation, as previously reported (44). Adding two-fold more or two-fold less Laurdan to the samples did not drastically change the spectra (Fig. S1), suggesting no notable effects of the probe. C-Laurdan and Pro12A dissolved in DMSO were added to biomimetic lipid-only samples after nanodisc formation at a molar ratio of 200:1 lipid to dye. The amount of DMSO added to samples was negligible (≤0.2% v/v). Flipper-TR was added to lipid-only samples at a molar ratio of 200:1 lipid to Flipper-TR. For samples derived from HEK293 membranes, Laurdan, C-Laurdan, and Pro12A were added to samples at a concentration of 1.25 nmol/mg wet membrane mass; Flipper-TR was added at 0.38 nmol Flipper-TR/mg wet membrane mass. Minimal amount of solvent was added (≤1% v/v) to all HEK293-derived samples.

Fluorescence spectroscopy measurements

Steady-state emission spectra were acquired using a Fluorolog-3 spectrofluorometer (Model FL-1039; Jobin Yvon, Edison, NJ) equipped with a xenon arc lamp. Sample temperature was maintained using a Peltier thermocouple drive (Model F-3004, Jobin Yvon, Edison, NJ). Samples in quartz cuvettes were incubated at the desired temperature in the Peltier drive for 5 min before analysis. Sample incubation at a particular temperature was reduced to 3 min if the sample was already within 5°C. Laurdan and C-Laurdan were excited at 385 nm, whereas Pro12A was excited at 370 nm. Steady-state spectra were recorded in 1-nm steps with bandwidths of 1.2 nm for both the excitation and emission monochromators. Emitted fluorescence was normalized to the lamp intensity detected by a reference detector for all spectra. For each independent experiment, spectra were recorded in triplicate and then averaged.

Fluorescence spectral analysis

Laurdan general polarization (GP) was calculated as before (44):

Please cite this article in press as: Real Hernandez and Levental, Lipid packing is disrupted in copolymeric nanodiscs compared with intact membranes, Biophysical Journal (2023), https://doi.org/10.1016/j.bpj.2023.01.013

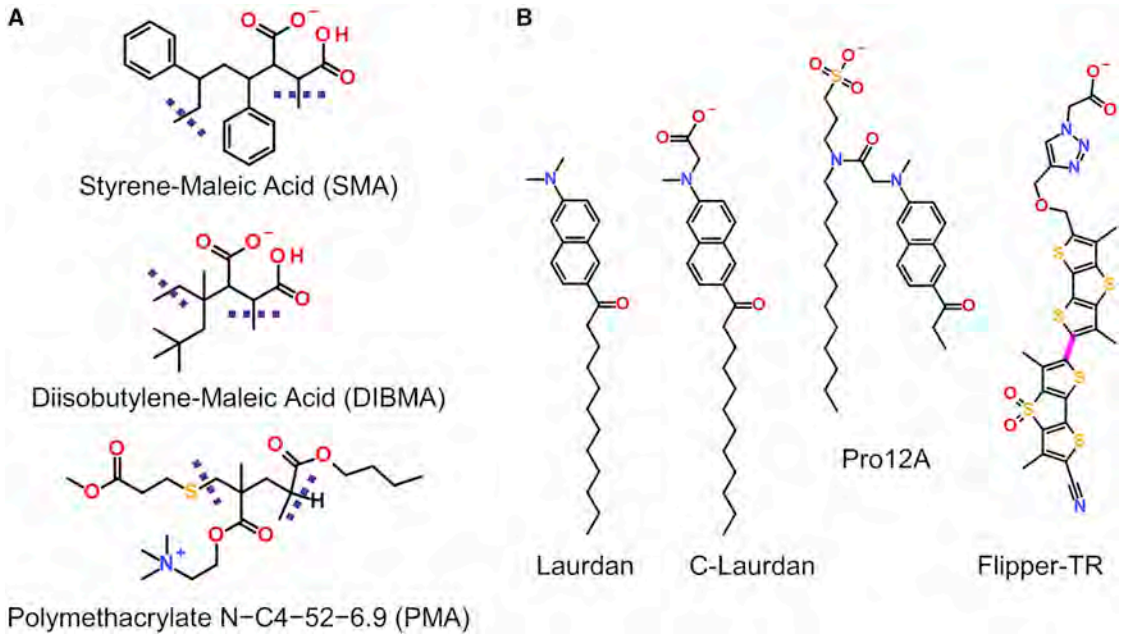

FIGURE 1 Chemical structures of copolymers used to form nanodiscs and fluorescent dyes used to measure membrane properties. (*A*) The copolymers used to form nanodiscs were SMA, DIBMA, and PMA. Dashed purple lines enclose the average repeating copolymeric unit of each copolymer strand. The SMA variant used had, on average, two styrene units for every one maleic acid unit (2:1). (*B*) Laurdan is composed of a 12-carbon aliphatic tail that embeds into lipid bilayers and a naphthalene-based chromophore that localizes near the glycerol-backbone of phospholipids in membranes. C-Laurdan and Pro12A have the same chromophore as Laurdan, but are charged at pH 7.4. C-Laurdan and Pro12A were used for comparison of Laurdan measurements made from biomimetic and biological membranes. Packing in the hydrophobic core of the membranes was measured using Flipper-TR fluorescence lifetime. Flipper-TR reports longer fluorescence lifetimes in membranes with higher lateral pressure (41). To see this figure in color, go online.

$$Laurdan\ GP = \frac{I_{440} - I_{490}}{I_{440} + I_{490}}$$

where I_{440} and I_{490} represent fluorescence emission intensity at 440 and 490 nm, respectively. The GP calculation for Laurdan was also used for C-Laurdan. For Pro12A excited at 370 nm, maximal fluorescence emission intensity in gel-phase (15°C) DMPC LUV was found to be at 432 nm, and in fluid-phase (33°C) DMPC LUV at 464 nm. Both wavelengths were used for Pro12 A GP calculation:

$$Pro12A\ GP = \frac{I_{432} - I_{464}}{I_{432} + I_{464}}$$

where I_{432} and I_{464} represent fluorescence emission intensity at 432 and 464 nm, respectively. Spectra were analyzed using Spectragryph (F. Menges "Spectragryph - optical spectroscopy software," Version 1.2.16.1, 2022, http://www.effemm2.de/spectragryph/). Significance was determined using a one-way ANOVA followed by a Bonferroni post hoc test.

Fluorescence lifetime imaging microscopy

Fluorescence lifetime imaging microscopy (FLIM) was used to measure the fluorescence lifetime of Flipper-TR in nanodiscs. FLIM images were taken on a Leica Microsystems TCS SP8 confocal microscope (Wetzlar, Germany) equipped with a pulsed white-light laser (WLL) operating at 80 MHz and time-gated hybrid detectors (HyD). Samples were imaged at 23°C in multi-well glass-bottom dishes (Matsunami Glass USA, Bellingham, WA), and they were illuminated using a 10×/0.40 air objective lens. All samples were excited at 488 nm and 575-625-nm emitted photons were collected. To diminish acquiring signal from sample interacting with the glass at the bottom of the dish, the focal plane was always set >300 μm above the surface of the glass. Collected images were 400 × 400 μm with a pixel size of 1.6 × 1.6 μm. Pixel dwell time was 30.78 μs, and collected photons were always >100,000 kCounts per image. Leica LAS X software was used to fit fluorescence decay data to a dual exponential model using its re-convolution function ($1.0 \leq \chi^2 \leq 1.2$). The longer lifetime component obtained is associated with lateral membrane pressure (41), and this component was averaged across all fields of view for a given sample.

RESULTS AND DISCUSSION

To investigate whether the lipid headgroup packing of intact membranes is retained in nanodiscs, we relied on the widely used and extensively characterized fluorescent membrane probe Laurdan and its analogues (38,39). Laurdan is an indirect sensor of lipid headgroup packing whose photophysical properties are affected by the polarity (i.e., relative hydration) of its local nano-environment (45). The most widely used manifestation of this effect is the red shift of Laurdan's fluorescence emission spectrum in loosely packed membranes, in which Laurdan interacts with more water molecules (45,46). This behavior is quantified as a GP, a dimensionless ratio of intensity of two different emission wavelengths (see section "materials and methods"), where higher values are correlated with more tightly packed lipid headgroups (44). In the following sections, we compare Laurdan's emission spectra (summarized by GP) in copolymeric nanodiscs to intact lipid bilayers composed of various lipid compositions, ranging from pure DMPC to biological membranes.

Please cite this article in press as: Real Hernandez and Levental, Lipid packing is disrupted in copolymeric nanodiscs compared with intact membranes, Biophysical Journal (2023), https://doi.org/10.1016/j.bpj.2023.01.013

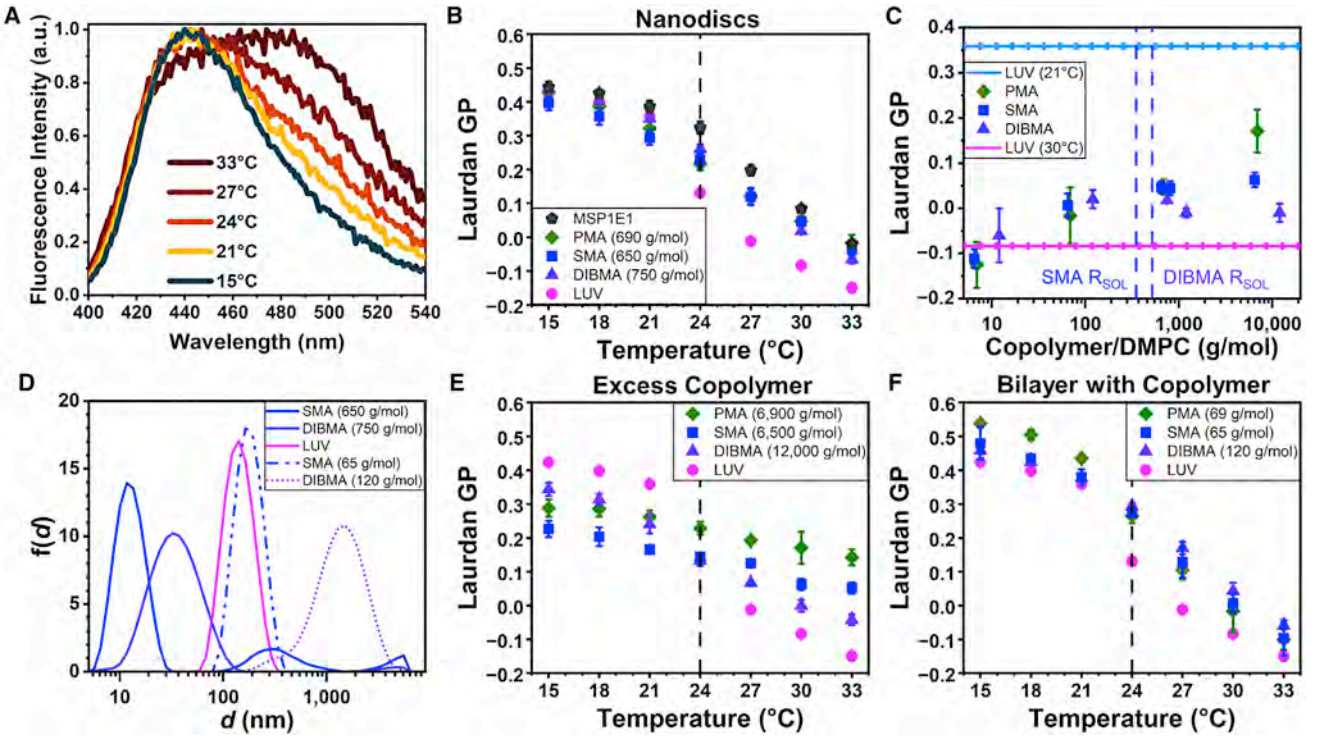

FIGURE 2 DMPC nanodiscs have higher Laurdan GP than LUVs above the melting point of DMPC. (*A*) Representative change in normalized Laurdan fluorescence emission spectra in SMA nanodiscs across the melting point of DMPC. Similar results were found for DIBMA and PMA nanodiscs. (*B*) Comparison of Laurdan GP in unperturbed DMPC LUV bilayers with those of copolymer- or MSP1E1-stabilized nanodiscs. (*C*) Laurdan GP of DMPC bilayers incubated with different amounts of copolymers analyzed at 30°C (i.e., above the melting point of DMPC $T_m = 24°C$). *Dashed vertical lines* indicate R_{SOL} values, which are the minimal copolymer-to-lipid ratios necessary to fully solubilize a membrane into nanodiscs. Laurdan GP of LUVs at 21°C (cyan) and 30°C (*pink*) are shown for reference. (*D*) Intensity-weighted particle size distributions ($f(d)$) of hydrodynamic diameter (d) for samples prepared below and above known R_{SOL} values (SMA $R_{SOL} = 350$ g/mol, DIBMA $R_{SOL} = 520$ g/mol). (*E* and *F*) Laurdan GP in copolymeric samples with excess copolymer to form nanodiscs (*E*) and with insufficient copolymer to form nanodiscs (*F*). Copolymer mass to DMPC molar ratio used for each sample indicated in legend. Melting point of DMPC ($T_m = 24°C$) referenced as black dashed line. Copolymer samples (SMA, DIBMA, and PMA) analyzed as independent triplicates ($n = 3$, mean ± SD). Membrane scaffold protein-stabilized nanodiscs (MSP1E1 ND) analyzed as independent duplicates ($n = 2$, mean ± SD). To see this figure in color, go online.

Nanodiscs have higher Laurdan GP than liposomes for fluid DMPC

We initially investigated pure DMPC bilayers as highly simplified models of biological lipid bilayers because DMPC has been widely used for structural studies of proteins embedded in nanodiscs (40,47). An example of the thermotropic behavior of DMPC in SMA-scaffolded nanodiscs is shown in Fig. 2 *A*. Nanodiscs scaffolded by DIBMA and PMA both show similar behaviors (Fig. S1 *A* and *B*). For DMPC, and almost all other nanodiscs/membranes analyzed, Laurdan's fluorescence emission spectra shift with temperature, displaying red-shifted fluorescence characteristic of more loosely packed lipids at higher temperatures. This behavior is fully expected, as lipids generally become less packed at higher temperatures (48,49). More specifically, DMPC has a gel-to-fluid transition temperature (T_m) at 24°C, which is evident in the notable transition in Laurdan GP of DMPC LUV at 24°C (Fig. 2 *B*). We observed a significant and consistent effect of embedding lipids into copolymeric nanodiscs: for all copolymers, lipid packing of DMPC was notably higher than for DMPC LUV at temperatures above DMPC's melting point. The same was true for all polymeric scaffolds (SMA, DIBMA, and PMA) and for MSP1E1-scaffolded nanodiscs (Fig. 2 *B*).

Another notable divergence between LUVs and nanodiscs was the lack of the sharp transition in Laurdan GP values around T_m in nanodiscs, suggesting reduced cooperativity between lipids. Similar loss of cooperativity has previously been reported by Laurdan and differential scanning calorimetry (DSC) for SMA-scaffolded nanodiscs with slightly different lipids (50). These observations suggest several conclusions: 1) the general thermotropic response of Laurdan indicates that it resides in, and reports on, the properties of nanodisc lipid bilayers; 2) the cooperative behavior of lipids is disrupted in nanodiscs; 3) fluid-phase bilayers in nanodiscs have more tightly packed lipid headgroups than intact liposomes. Moreover, since SMA, DIBMA, and MSP1E1 scaffolds have very different hydrophobic moieties embedded in the lipid bilayer and form nanodiscs via different mechanisms, we propose that these phenomena may be generalizable to other nanodisc preparations.

To determine if the copolymer-induced increase in lipid packing is dependent on copolymer-to-lipid ratios, we

Please cite this article in press as: Real Hernandez and Levental, Lipid packing is disrupted in copolymeric nanodiscs compared with intact membranes, Biophysical Journal (2023), https://doi.org/10.1016/j.bpj.2023.01.013

TABLE 1 Z-Average sizes and PDI of DMPC LUV or nanodiscs

	Copolymer-to-lipid ratio (g/mol DMPC)	Z-Average size (nm)	PDI
LUV	–	133	0.08
SMA	65	169	0.07
	650	15	0.38
DIBMA	120	1080	0.29
	750	30	0.31

analyzed Laurdan GP in DMPC LUV incubated with increasing amounts of copolymer (Fig. 2 *C*). Samples were analyzed at 30°C (i.e., above DMPC melting temperature). A relevant reference parameter here is R_{SOL}, which represents the minimal copolymer amount required to completely transform all LUV bilayers into nanodiscs. R_{SOL} values (350 g/mol DMPC for SMA; 520 g/mol DMPC for DIBMA), were previously determined using solution-based phosphorus (^{31}P) NMR (30,51), and are represented in Fig. 2 *B* as dashed vertical lines. Low copolymer ratios (<20 g/mol lipid; order of magnitude below R_{SOL}) did not significantly affect Laurdan GP (Fig. 2 *C*), presumably because the copolymer in the bilayer is too dilute to significantly perturb lipid organization. At 60–120 g/mol lipid, still well below the solubilizing concentration R_{SOL}, both SMA and DIBMA already increased Laurdan GP, indicating that the effects on membrane bilayer structure are driven by lipid-copolymer interactions, rather than transformation into nanodiscs. SMA, DIBMA, and PMA at concentrations beyond R_{SOL} all significantly increased Laurdan GP, suggesting more tightly packed lipid headgroups in these nanodiscs relative to unperturbed membranes.

To confirm that samples prepared at copolymer concentrations of 650–750 g/mol contain nanodiscs, we used DLS to determine particle sizes (Fig. 2 *D*). SMA (650 g/mol lipid) produced 15-nm particles, whereas DIBMA (750 g/mol lipid) produced 30-nm particles (Table 1), both consistent with the previously reported sizes of their respective nanodiscs (30,52). Samples prepared with 10-fold less copolymer did not contain particles smaller than 50 nm, but did contain particles larger than untreated LUVs. This enlargement of liposomes below solubilizing concentrations may be due to copolymer strands incorporating into the bilayers.

In the presence of excess copolymer (>6000 g/mol lipid), far beyond reported R_{SOL} values, we observed major disruptions to membrane behavior, with copolymer mixtures showing no evidence of a transition at the DMPC T_m, much lower Laurdan GP values than LUVs at low temperatures, and much higher Laurdan GP values at higher temperatures (Fig. 2 *E*). These results suggest that high copolymer-to-lipid ratios may produce non-bilayer-like structures (e.g., mixed lipid-copolymer micelles), and therefore that caution is required to avoid excessive copolymer during membrane protein isolation. Consistently, excess SMA has been found to increase solubilization of rhodopsin, but render it inactive (53). Increased Laurdan GP values above the melting point of DMPC were also observed in samples prepared with relatively low copolymer concentrations (Fig. 2 *F*), indicating that the observed bilayer effects occur before nanodisc formation, potentially due to significant fraction of lipids in intact bilayers already interacting with the copolymer. At very low copolymer amounts (<20 g/mol lipid), no significant effects on bilayer properties are observed by Laurdan (Fig. S2).

Fluid POPC-DPPC bilayers have significantly higher Laurdan GP in copolymeric nanodiscs

The above results reveal that, for DMPC, copolymeric nanodiscs have significantly increased lipid headgroup packing relative to liposomes at temperatures where the lipid is expected to be in the fluid phase. To determine if these effects persist in more complex, multi-component bilayers capable of phase coexistence, we measured Laurdan GP in nanodiscs made from mixtures of POPC and DPPC. These two lipids were selected because 1) they represent common lipid species in mammalian membranes (54,55), 2) their mixtures have a well-defined phase diagram (56), and 3) their gel-to-fluid-phase T_m are very different (DPPC = 41°C, POPC = −2°C), allowing us to evaluate situations wherein one lipid species is above and the other is below its T_m (i.e., expected fluid and gel phases, respectively, in unperturbed membranes).

POPC-DPPC mixtures were analyzed at 20°C, where their phase behavior depends on DPPC concentration, and 60°C, where it does not (see Fig. 3 *A*, replotted from published data) (56). That is, all POPC-DPPC mixtures are fluid at 60°C, whereas, at 20°C, membranes containing ∼20%–80% DPPC produce coexisting DPPC-rich gel and POPC-rich fluid phases. All copolymer nanodisc samples analyzed in this study were formed at a temperature above the melting points of all phospholipids (i.e., 60°C for POPC-DPPC mixtures) to avoid preferential solubilization of different lipid phases. At 60°C, SMA and PMA significantly increased Laurdan GP for all POPC-DPPC mixtures (Fig. 3 *B*). The magnitude of the effect was similar for SMA and PMA, and somewhat smaller for DIBMA; i.e., Laurdan GP in DIBMA nanodiscs was most similar to LUVs (Fig. 3 *B*). This effect was also observed for several DMPC samples (see Fig. 2). These observations suggest that DIBMA perturbs the typical bilayer arrangement of DMPC lipids less than the other two scaffolds (SMA and PMA). One possible explanation is that DIBMA's hydrophobic moiety is aliphatic rather than aromatic (as for SMA), making it more similar to, and less perturbing of, the aliphatic chemistry of lipid acyl chains (52). On the other hand, PMA also has an aliphatic moiety but has effects on lipid packing similar to SMA. Another distinguishing feature of DIBMA relative to PMA and SMA is that it forms slightly larger nanodiscs (57), as validated by our DLS measurements (Fig. 2 *C*). Thus, nanodisc size may determine the extent of lipid perturbation in

Please cite this article in press as: Real Hernandez and Levental, Lipid packing is disrupted in copolymeric nanodiscs compared with intact membranes, Biophysical Journal (2023), https://doi.org/10.1016/j.bpj.2023.01.013

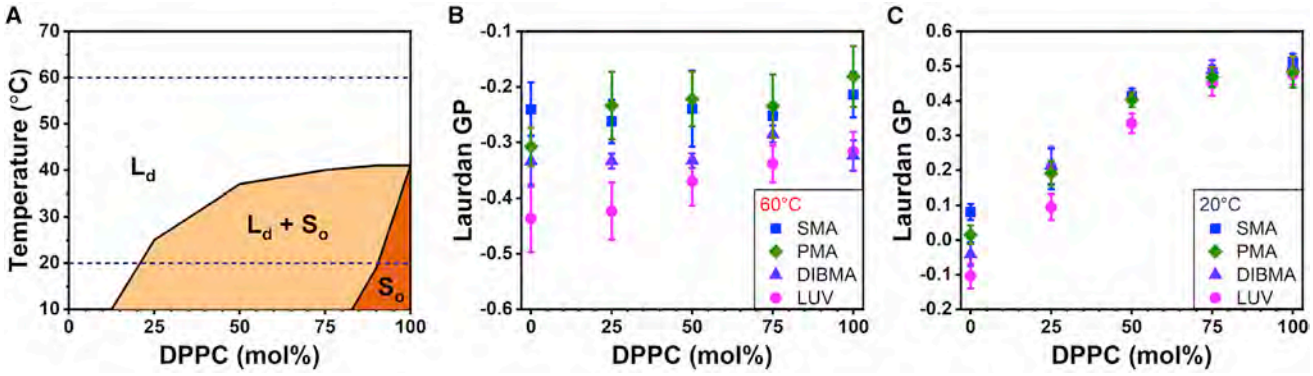

FIGURE 3 Copolymers increase Laurdan GP of POPC-DPPC bilayers, with larger effects on more fluid bilayers. (*A*) Phase diagram of POPC-DPPC mixtures replotted from published data (56). Regions of fluid (L_d), gel (S_o), and coexisting phases ($L_d + S_o$) labeled. Dashed lines indicate temperatures at which mixtures were analyzed. (*B* and *C*) Laurdan GP of POPC-DPPC mixtures at 60°C (*B*) or 20°C (*C*). All samples analyzed as independent experimental triplicates ($n = 3$, mean ± SD). All samples prepared at: 650 g SMA/mol lipid, 1200 g DIBMA/mol lipid, or 690 g PMA/mol lipid. To see this figure in color, go online.

nanodiscs, as has previously been suggested (58). However, it is important to emphasize that even the least-perturbing scaffold still generally produces nanodiscs with different membrane properties than in liposomes.

At 60°C, Laurdan GP for these mixtures was not strongly dependent on composition, as both POPC and DPPC are fluid at this temperature. In contrast, at 20°C, Laurdan GP was strongly dependent on DPPC concentration, both in LUVs and nanodiscs (Fig. 3 *C*), very likely because DPPC is below its T_m and, therefore, tends to form ordered, tightly packed bilayers. Higher GP values in DPPC-rich mixtures suggest a higher fraction of lipids in relatively ordered states. In LUVs, the ordered state is a gel phase (56). In nanodiscs, conceptions of phases are complicated by each bilayer leaflet only containing a few hundred lipids (59). Despite this caveat, the similarity in GP values between LUVs and nanodiscs at 20°C for various DPPC-containing mixtures suggests the surprising inference that nanodiscs can retain similar membrane states as unperturbed liposomes. All copolymers significantly increased Laurdan GP when a major fraction of lipids are expected to be in a fluid state (i.e., POPC ≥ 50 mol %), with the magnitude of the effect apparently related to the fraction of fluid (relative to ordered) membrane (Fig. 3 *C*). This observation is consistent with our previous conclusion that relatively disordered membranes are most susceptible to perturbation by copolymers in nanodiscs.

Liquid-disordered biomimetic bilayers have increased Laurdan GP values in copolymeric nanodiscs

Mammalian cell membranes are thought to be almost exclusively in fluid phases (60,61). However, although they generally do not contain gel phases, they are believed to be capable of forming lateral membrane heterogeneities of increased lipid order (62). Such regions are known as lipid rafts, and arise due to preferential interactions between cholesterol and saturated phospho- and sphingo-lipids (63). In model membranes, this capacity for lateral liquid domains can be modeled by mixtures containing sterols, low-melting phospholipids, and high-melting phospholipids, which tend to form coexisting ordered and disordered fluid phases, with the liquid-ordered phase hypothetically mimicking the molecular architecture of cellular lipid rafts (64). To test the effect of copolymer scaffolds on lipid compositions simulating mammalian plasma membranes, we compared LUVs with nanodiscs containing mixtures of POPC, PSM, and cholesterol. The phase behavior of these mixtures at physiological temperature (37°C) has been defined (65), and we tested representative ternary mixtures that form either single-phase liquid-disordered (L_d), single-phase liquid-ordered (L_o), or a mixture of the two phases ($L_d + L_o$) in liposomes at 37°C.

For L_d membranes, the effects of copolymer scaffolding were similar to those reported above: all copolymer membranes had higher Laurdan GP, with the smallest effect for DIBMA (Fig. 4 *A*). Interestingly, pure L_o bilayers were essentially unaffected in nanodiscs, retaining the high Laurdan GP of intact liposomes. This observation was consistent with the minimal effects of nanodisc encapsulation on ordered DPPC-rich bilayers (Fig. 3 *C*). For bilayers with coexisting L_d and L_o phases, we observed an intermediate effect: a small, but clear increase in Laurdan GP in nanodiscs. These observations were similar when samples were analyzed at 25°C (Fig. S3) (65). Thus, even though L_o bilayers are fluid and not gel, copolymeric nanodiscs appear to minimally perturb these highly ordered bilayers. This observation suggests that copolymeric nanodiscs may faithfully recapitulate headgroup packing for membranes mimicking lipid rafts, which are believed to be represented by L_o phases (66). However, although lipid packing assayed by Laurdan is well maintained in these highly ordered bilayers, it will be important to ensure that other relevant biophysical properties are similar unaffected by copolymers.

Please cite this article in press as: Real Hernandez and Levental, Lipid packing is disrupted in copolymeric nanodiscs compared with intact membranes, Biophysical Journal (2023), https://doi.org/10.1016/j.bpj.2023.01.013

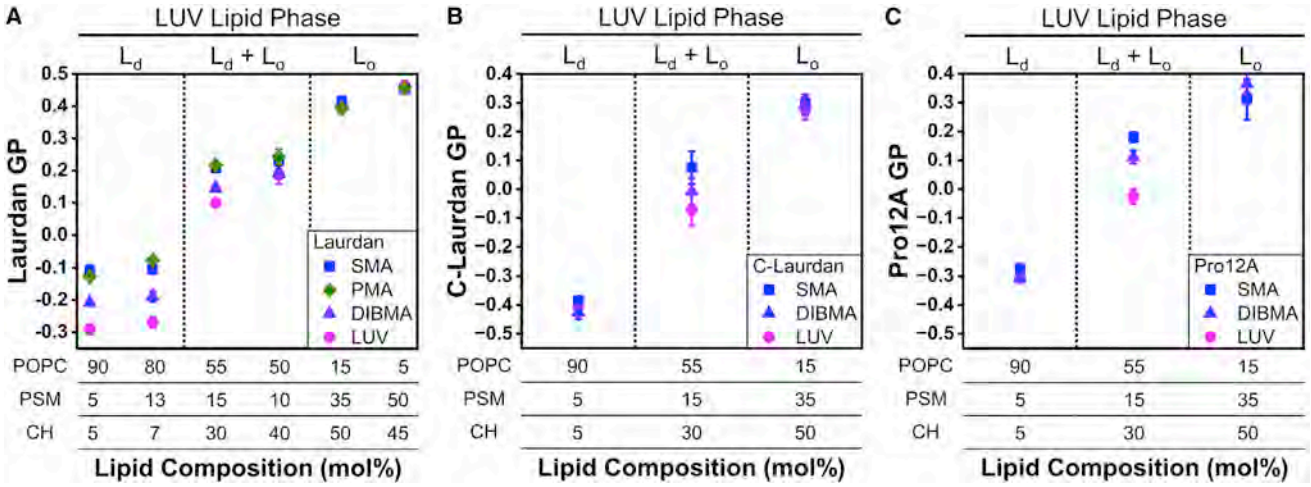

FIGURE 4 Laurdan GP is increased by copolymeric scaffolds in fluid-disordered lipid bilayers, but least affected by DIBMA. (*A*) Lipid headgroup packing measured by Laurdan GP in representative mixtures that show single-phase L_d, single-phase L_o, or coexisting $L_d + L_o$ phases in LUV membranes. For each LUV phase scenario, two representative lipid compositions were analyzed. (*B* and *C*) GP values of selected lipid compositions analyzed by C-Laurdan (*B*) or Pro12A (*C*). Lipid compositions in columns shown as molar percentage of 1-palmitoyl-2-oleoyl-phosphocholine (POPC), palmitoyl-sphingomyelin (PSM), and cholesterol (CH). LUV lipid phase (fluid disordered, L_d; fluid ordered, L_o) determined from published phase diagram (65). Nanodiscs were formed at 650 g SMA/mol lipid, 1200 g DIBMA/mol lipid, or 690 g PMA/mol lipid. All samples analyzed at 37°C as independent triplicates ($n = 3$, mean ± SD). To see this figure in color, go online.

Although Laurdan can robustly report on lipid headgroup packing, analogous dyes with different chemical structures can also be used to measure membrane properties (39,67). Such dyes include C-Laurdan and Pro12A (Fig. 1 *B*), among many others (68). To determine whether other environment-sensitive fluorophores would also report differences in physical properties between copolymeric nanodiscs and liposomes, the GP values of C-Laurdan and Pro12A were compared between LUVs and nanodiscs composed of cholesterol-containing mixtures. GP values in L_o bilayers were similar between nanodiscs and LUVs analyzed with C-Laurdan and Pro12A (Fig. 4 *B* and *C*), similar to observations with Laurdan (Fig. 4 *A*). For bilayers with coexisting $L_d + L_o$ phases, a notable increase in GP values was observed in nanodiscs, with DIBMA being less perturbing than SMA, again agreeing with Laurdan observations in the same lipid composition (Fig. 4 *A*) and in DPPC-POPC mixtures (Fig. 3 *C*). Interestingly, unlike with Laurdan, C-Laurdan and Pro12A did not show increased GP for L_d bilayers in nanodiscs (Fig. 4 *B* and *C*). This was an unexpected result, given that Laurdan systematically showed increased GP values for fluid bilayers in copolymeric nanodiscs (Figs. 2 *C* and 3 *B*). One possible explanation for this discrepancy may be that C-Laurdan and Pro12A are negatively charged at our conditions, and would therefore be repelled by the negatively charged maleic acid moieties of SMA and DIBMA (Fig. 1). In this case, these reporters may be distributed preferentially to more central regions of copolymeric nanodiscs where lipid headgroup packing/hydration may be less perturbed than at the copolymer-lipid bilayer interface (69). The presence of heterogeneous lipid environments inside nanodiscs has been well documented (69,70), so it is possible that regions with low membrane perturbation coexist with highly perturbed membrane regions.

Biological membrane lipids have increased lipid headgroup packing in copolymeric nanodiscs

The synthetic bilayers analyzed above have contained only lipids, but biological membranes include a high fraction of proteins, estimated up to 20% area fraction (71). Amphiphilic copolymers can isolate membrane proteins directly from membranes for studies of their structure and function (72–74), and it may be a tempting assumption that resulting copolymeric nanodiscs retain a protein's native membrane environment (75–77). Our data in lipid-only nanodiscs do not support this assumption. To determine whether lipid headgroup packing is retained in copolymeric nanodiscs derived from biological membranes, we compared isolated HEK293 membranes with copolymeric nanodiscs made from those membranes. HEK293 cells were selected because these have been used for SMA-mediated isolation of membrane proteins (78,79). A standard method for producing copolymeric nanodiscs from biological membranes has been published (43), but this protocol may involve the use of excess copolymer (2.5% w/v or 25 g/L) during nanodisc formation (42). Excess copolymer strongly perturbs membrane properties (Fig. 2 *E*) and membrane protein function (80). For our studies, we used 1 mg of copolymer per gram of HEK293 membrane for nanodisc formation to avoid excess copolymer (42), and then removed any undissolved membrane material by centrifugation.

For all three dyes referenced above, we observed higher GP values relative to intact membranes in copolymeric nanodiscs made from isolated HEK293 membranes at 37°C

Please cite this article in press as: Real Hernandez and Levental, Lipid packing is disrupted in copolymeric nanodiscs compared with intact membranes, Biophysical Journal (2023), https://doi.org/10.1016/j.bpj.2023.01.013

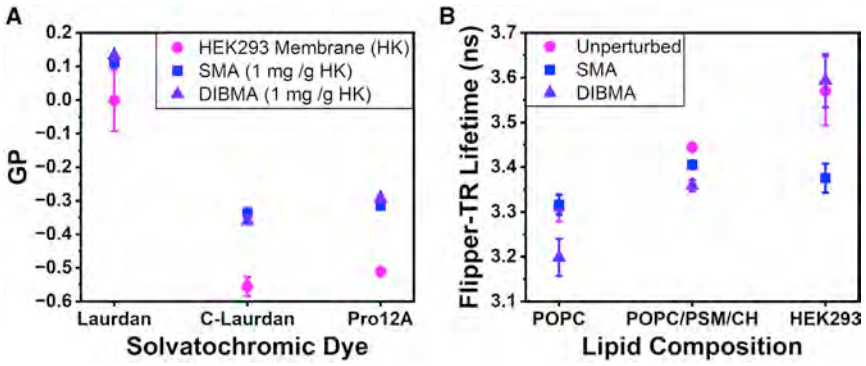

FIGURE 5 GP increases in copolymeric nanodiscs prepared from mammalian cell membranes, but lateral pressure decreases in SMA nanodiscs. (*A*) GP values of various solvatochromic dyes in nanodiscs prepared from HEK293 membranes. All samples analyzed as independent triplicates ($n = 3$, mean ± SD). (*B*) Flipper-TR fluorescence lifetime in nanodiscs. For pure POPC bilayers, SMA samples were prepared at 1300 g/mol lipid and DIBMA samples at 2400 g/mol lipid. For bilayers containing POPC, PSM, and cholesterol (CH), SMA samples were prepared at 650 g/mol and DIBMA samples at 1200 g/mol. HEK293 nanodiscs were prepared with 1 mg of copolymer per gram of wet HEK293 membrane mass (1 mg/g HK). "Unperturbed" refers to membrane unexposed to copolymer. Each point represents the average lifetime collected from independent experiments analyzed with at least five different frames of view ($n = 3$, mean ± SEM). Samples analyzed at 37°C, pH = 7.4. To see this figure in color, go online.

(Fig. 5 *A*). In contrast to lipid-only membranes (Figs. 3 *B* and 4 *A*), DIBMA perturbs lipid packing similarly to SMA. These observations suggest that copolymeric scaffolds also increase lipid ordering for protein-rich membranes.

All solvatochromic dyes referenced above change their spectra in membranes due to dipolar relaxation via the water molecules hydrating their surrounding polar lipid headgroups. Tighter headgroup packing reduces hydration levels, which reduces dipolar relaxation and leads to blue-shifted spectra (i.e., higher GP) (39). To determine whether reporters not dependent on dipolar relaxation would also behave differently in nanodiscs relative to unperturbed membranes, we analyzed the fluorescence lifetime of Flipper-TR. Flipper-TR reports on lipid packing/lateral pressure within the hydrophobic bilayer core, via the dependence of its fluorescence emission lifetime on the degree of planarization of its two flexible dithienothiophene moieties (Fig. 1 *B*) (41). We compared Flipper-TR lifetimes in intact bilayers versus copolymer nanodiscs for POPC, a ternary lipid mixture, and isolated HEK membranes (Fig. 5 *B*). Although the effects were more heterogeneous than for Laurdan, there was a general trend that nanodiscs showed somewhat lower fluorescence lifetimes (reduced acyl chain pressure) in nanodiscs compared with intact bilayers (Fig. 5 *B*). The largest reduction was observed for SMA-solubilized HEK membranes. This effect was somewhat surprising, as we expected increased headgroup packing (reported by Laurdan) to correlate with increased packing/pressure in the hydrophobic core (reported by Flipper-TR). These observations tentatively suggest that, in copolymer-stabilized nanodiscs, packing of lipid acyl chains may be somewhat decoupled from packing of lipid headgroups. Ultimately, although the structural details of lipid bilayers in copolymer nanodiscs remain to be fully characterized, they appear to be broadly different from those of intact membranes.

CONCLUSIONS

Nanodiscs have become an invaluable tool for studies of membrane protein structure and function, but their deviations from unperturbed membrane structure should be considered. The strongest effect presented in this study is that lipid headgroup packing is perturbed in copolymeric nanodiscs relative to intact membranes. In lipid-only nanodiscs, the copolymer DIBMA was less perturbing than SMA or PMA, but still changed membrane properties compared with intact bilayers. Although we focus mostly on one property of bilayer membranes (lipid packing), other membrane properties that are expected to correlate with lipid packing (fluidity, rigidity) may also be perturbed. Another common property of biomembranes likely disrupted in nanodiscs is lipid asymmetry between the leaflets of the bilayers (81). Even if asymmetry is maintained during the original extraction of lipids, copolymeric nanodiscs are known to rapidly exchange lipids via inter-nanodisc collisions (82,83), which would likely allow mixing of bilayer leaflets and loss of compositional asymmetry. Altogether, these results suggest that, although copolymeric nanodiscs can be composed of native membrane lipids, they generally do not retain the physical properties of the membranes from which they are derived.

SUPPORTING MATERIAL

Supporting material can be found online at https://doi.org/10.1016/j.bpj.2023.01.013.

AUTHOR CONTRIBUTIONS

I.L. conceived and supervised the project. L.M.R.H. conducted the experiments and analyzed the data. I.L. and L.M.R.H. wrote and edited the manuscript.

ACKNOWLEDGMENTS

We would like to thank Steve Reichow's laboratory at Portland State University for supplying the MSP1E1 DMPC nanodiscs used in this study, the lab of Andrey Klymchenko for gifting us the dye Pro12A, and members of the Levental lab for discussions and input. Funding for this work was provided by the NIH/National Institute of General Medical Sciences (GM134949, GM120351), the Volkswagen Foundation (grant 93091), and the Human Frontier Science Program (RGP0059/2019).

Please cite this article in press as: Real Hernandez and Levental, Lipid packing is disrupted in copolymeric nanodiscs compared with intact membranes, Biophysical Journal (2023), https://doi.org/10.1016/j.bpj.2023.01.013

DECLARATION OF INTERESTS

The authors declare no competing interests.

REFERENCES

1. Fagerberg, L., K. Jonasson, …, L. Berglund. 2010. Prediction of the human membrane proteome. *Proteomics.* 10:1141–1149.
2. Uhlén, M., L. Fagerberg, …, F. Pontén. 2015. Tissue-based map of the human proteome. *Science.* 347:1260419.
3. Sriram, K., and P. A. Insel. 2018. G protein-coupled receptors as targets for approved drugs: how many targets and how many drugs? *In* Molecular Pharmacology American Society for Pharmacology and Experimental Therapy, pp. 251–258.
4. Choy, B. C., R. J. Cater, …, E. E. Pryor. 2021. A 10-year meta-analysis of membrane protein structural biology: detergents, membrane mimetics, and structure determination techniques. *Biochim. Biophys. Acta Biomembr.* 1863:183533.
5. Hardy, D., E. Desuzinges Mandon, …, A. Jawhari. 2018. The yin and yang of solubilization and stabilization for wild-type and full-length membrane protein. *Methods.* 147:118–125.
6. Chipot, C., F. Dehez, …, P. Schanda. 2018. Perturbations of native membrane protein structure in alkyl phosphocholine detergents: a critical assessment of NMR and biophysical studies. *Chem. Rev.* 118:3559–3607.
7. Zoghbi, M. E., R. S. Cooper, and G. A. Altenberg. 2016. The lipid bilayer modulates the structure and function of an ATP-binding cassette exporter. *J. Biol. Chem.* 291:4453–4461.
8. Renard, K., and B. Byrne. 2021. Insights into the role of membrane lipids in the structure, function and regulation of integral membrane proteins. *Int. J. Mol. Sci.* 22:9026.
9. Levental, I., and E. Lyman. 2022. Regulation of membrane protein structure and function by their lipid nano-environment. *Nat Rev Mol Cell Biol*. https://doi.org/10.1038/s41580-022-00524-4.
10. Manna, M., M. Niemelä, …, I. Vattulainen. 2016. Mechanism of allosteric regulation of β2-adrenergic receptor by cholesterol. *Elife.* 5:e18432.
11. Jaipuria, G., A. Leonov, …, M. Zweckstetter. 2017. Cholesterol-mediated allosteric regulation of the mitochondrial translocator protein structure. *Nat. Commun.* 8:14893–14898.
12. Huang, S. K., O. Almurad, …, R. S. Prosser. 2022. Allosteric modulation of the adenosine A2A receptor by cholesterol. *Elife.* 11:e73901.
13. Anderluh, A., T. Hofmaier, …, G. J. Schütz. 2017. Direct PIP 2 binding mediates stable oligomer formation of the serotonin transporter. *Nat. Commun.* 8:14089.
14. Stefanski, K. M., C. M. Russell, …, F. N. Barrera. 2021. PIP2promotes conformation-specific dimerization of the EphA2 membrane region. *J. Biol. Chem.* 296:100149.
15. Chadda, R., N. Bernhardt, …, J. L. Robertson. 2021. Membrane transporter dimerization driven by differential lipid solvation energetics of dissociated and associated states. *Elife.* 10:e63288.
16. Halbleib, K., K. Pesek, …, R. Ernst. 2017. Activation of the unfolded protein response by lipid bilayer stress. *Mol. Cell.* 67:673–684.e8.
17. Covino, R., S. Ballweg, …, R. Ernst. 2016. A eukaryotic sensor for membrane lipid saturation. *Mol. Cell.* 63:49–59.
18. Strickland, K. M., K. Neselu, …, I. Schmidt-Krey. 2021. Reconstitution of detergent-solubilized membrane proteins into proteoliposomes and nanodiscs for functional and structural studies. *In* Methods in Molecular Biology Humana Press Inc., pp. 21–35.
19. Ando, M., S. Schikula, …, K. Akiyoshi. 2018. Proteoliposome engineering with cell-free membrane protein synthesis: control of membrane protein sorting into liposomes by chaperoning systems. *Adv. Sci.* 5:1800524.
20. Amati, A. M., S. Graf, …, C. von Ballmoos. 2020. Current problems and future avenues in proteoliposome research. *Biochem. Soc. Trans.* 48:1473–1492.
21. Hugentobler, K. G., D. Heinrich, …, S. Block. 2020. Lipid composition affects the efficiency in the functional reconstitution of the cytochrome c oxidase. *Int. J. Mol. Sci.* 21:6981–7017.
22. Denisov, I. G., and S. G. Sligar. 2017. Nanodiscs in membrane biochemistry and biophysics. *Chem. Rev.* 117:4669–4713.
23. Bayburt, T. H., Y. V. Grinkova, and S. G. Sligar. 2002. Self-assembly of discoidal phospholipid bilayer nanoparticles with membrane scaffold proteins. *Nano Lett.* 2:853–856.
24. Civjan, N. R., T. H. Bayburt, …, S. G. Sligar. 2003. Direct solubilization of heterologously expressed membrane proteins by incorporation into nanoscale lipid bilayers. *Biotechniques.* 35:556–562.
25. Inagaki, S., R. Ghirlando, and R. Grisshammer. 2013. Biophysical characterization of membrane proteins in nanodiscs. *Methods.* 59:287–300.
26. Denisov, I. G., and S. G. Sligar. 2016. Nanodiscs for structural and functional studies of membrane proteins. *Nat. Struct. Mol. Biol.* 23:481–486.
27. Orwick, M. C., P. J. Judge, …, A. Watts. 2012. Detergent-free formation and physicochemical characterization of nanosized lipid-polymer complexes: Lipodisq. *Angew. Chem., Int. Ed. Engl.* 51:4653–4657.
28. Malhotra, K., and N. N. Alder. 2014. Advances in the use of nanoscale bilayers to study membrane protein structure and function. *Biotechnol. Genet. Eng. Rev.* 30:79–93.
29. Scheidelaar, S., M. C. Koorengevel, …, J. A. Killian. 2015. Molecular Model for the solubilization of membranes into nanodisks by styrene maleic acid copolymers. *Biophys. J.* 108:279–290.
29. Grethen, A., A. O. Oluwole, S. Keller…, 2017. Thermodynamics of nanodisc formation mediated by styrene/maleic acid (2:1) copolymer. *Sci. Rep.* 7, 11517.
31. Xue, M., L. Cheng, …, S. J. Marrink. 2018. Molecular mechanism of lipid nanodisk formation by styrene-maleic acid copolymers. *Biophys. J.* 115:494–502.
32. Scheidelaar, S., M. C. Koorengevel, …, J. A. Killian. 2016. Effect of polymer composition and pH on membrane solubilization by styrene-maleic acid copolymers. *Biophys. J.* 111:1974–1986.
33. Bjørnestad, V. A., M. Orwick-Rydmark, and R. Lund. 2021. Understanding the structural pathways for lipid nanodisc formation: how styrene maleic acid copolymers induce membrane fracture and disc formation. *Langmuir.* 37:6178–6188.
34. Overduin, M., and M. Esmaili. 2019. Structures and interactions of transmembrane targets in native nanodiscs. *SLAS Discov.* 24:943–952.
35. Dörr, J. M., M. C. Koorengevel, …, J. A. Killian. 2014. Detergent-free isolation, characterization, and functional reconstitution of a tetrameric K+ channel: the power of native nanodiscs. *Proc. Natl. Acad. Sci. USA.* 111:18607–18612.
36. Teo, A. C. K., S. C. Lee, …, D. I. Roper. 2019. Analysis of SMALP co-extracted phospholipids shows distinct membrane environments for three classes of bacterial membrane protein. *Sci. Rep.* 9:1813.
36. Barniol-Xicota, M., and S. H. L. Verhelst. 2021. Lipidomic and in-gel analysis of maleic acid co-polymer nanodiscs reveals differences in composition of solubilized membranes. *Commun. Biol.* 4, 218.
38. Gunther, G., L. Malacrida, …, S. A. Sánchez. 2021. Laurdan since weber: the quest for visualizing membrane heterogeneity. *Acc. Chem. Res.* 54:976–987.
39. Danylchuk, D. I., E. Sezgin, …, A. S. Klymchenko. 2020. Redesigning solvatochromic probe laurdan for imaging lipid order selectively in cell plasma membranes. *Anal. Chem.* 92:14798–14805.
40. Flores, J. A., B. G. Haddad, …, S. L. Reichow. 2020. Connexin-46/50 in a dynamic lipid environment resolved by CryoEM at 1.9 Å. *Nat. Commun.* 11:1–11.
41. Colom, A., E. Derivery, …, A. Roux. 2018. A fluorescent membrane tension probe. *Nat. Chem.* 10:1118–1125.

Please cite this article in press as: Real Hernandez and Levental, Lipid packing is disrupted in copolymeric nanodiscs compared with intact membranes, Biophysical Journal (2023), https://doi.org/10.1016/j.bpj.2023.01.013

42. Kopf, A. H., J. M. Dörr, …, J. A. Killian. 2020. Factors influencing the solubilization of membrane proteins from Escherichia coli membranes by styrene–maleic acid copolymers. *Biochim. Biophys. Acta Biomembr.* 1862:183125.
43. Lee, S. C., T. J. Knowles, …, T. R. Dafforn. 2016. A method for detergent-free isolation of membrane proteins in their local lipid environment. *Nat. Protoc.* 11:1149–1162.
44. Amaro, M., F. Reina, …, E. Sezgin. 2017. Laurdan and Di-4-ANEPPDHQ probe different properties of the membrane. *J. Phys. D Appl. Phys.* 50:134004.
45. Parasassi, T., E. K. Krasnowska, …, E. Gratton. 1998. Laurdan and prodan as polarity-sensitive fluorescent membrane probes. *J. Fluoresc.* 8:365–373.
46. Parasassi, T., G. De Stasio, …, E. Gratton. 1991. Quantitation of lipid phases in phospholipid vesicles by the generalized polarization of Laurdan fluorescence. *Biophys. J.* 60:179–189.
46. Peter, M. F., J. A. Ruland, G. Hagelueken…, 2022. Structural and mechanistic analysis of a tripartite ATP-independent periplasmic TRAP transporter. *Nat. Commun.* 13, 4471.
48. Cossins, A. R., and C. L. Prosser. 1978. Evolutionary adaptation of membranes to temperature. *Proc. Natl. Acad. Sci. USA.* 75:2040–2043.
49. Cano-Ramirez, D. L., L. Carmona-Salazar, …, M. Gavilanes-Ruíz. 2021. Plasma membrane fluidity: an environment thermal detector in plants. *Cells.* 10:2778.
50. Dominguez Pardo, J. J., J. M. Dörr, …, J. A. Killian. 2017. Thermotropic properties of phosphatidylcholine nanodiscs bounded by styrene-maleic acid copolymers. *Chem. Phys. Lipids.* 208:58–64.
51. Cuevas Arenas, R., J. Klingler, …, S. Keller. 2016. Influence of lipid bilayer properties on nanodisc formation mediated by styrene/maleic acid copolymers. *Nanoscale.* 8:15016–15026.
52. Oluwole, A. O., B. Danielczak, …, S. Keller. 2017. Solubilization of membrane proteins into functional lipid-bilayer nanodiscs using a diisobutylene/maleic acid copolymer. *Angew. Chem., Int. Ed. Engl.* 56:1919–1924.
53. Pitch, S. G., W. Yao, …, D. L. Farrens. 2021. Functional integrity of membrane protein rhodopsin solubilized by styrene-maleic acid copolymer. *Biophys. J.* 120:3508–3515.
54. Symons, J. L., K. J. Cho, …, K. R. Levental. 2021. Lipidomic atlas of mammalian cell membranes reveals hierarchical variation induced by culture conditions, subcellular membranes, and cell lineages. *Soft Matter.* 17:288–297.
57. Levental, K. R., E. Malmberg, I. Levental…, 2020. Lipidomic and biophysical homeostasis of mammalian membranes counteracts dietary lipid perturbations to maintain cellular fitness. *Nat. Commun.* 11, 1339.
56. Svetlovics, J. A., S. A. Wheaten, and P. F. Almeida. 2012. Phase separation and fluctuations in mixtures of a saturated and an unsaturated phospholipid. *Biophys. J.* 102:2526–2535.
57. Voskoboynikova, N., E. G. Margheritis, …, K. Cosentino. 2021. Evaluation of DIBMA nanoparticles of variable size and anionic lipid content as tools for the structural and functional study of membrane proteins. *Biochim. Biophys. Acta Biomembr.* 1863:183588.
58. Gulamhussein, A. A., R. Uddin, …, A. J. Rothnie. 2020. A comparison of SMA (styrene maleic acid) and DIBMA (di-isobutylene maleic acid) for membrane protein purification. *Biochim. Biophys. Acta Biomembr.* 1862:183281.
59. Shaw, A. W., M. A. McLean, and S. G. Sligar. 2004. Phospholipid phase transitions in homogeneous nanometer scale bilayer discs. *FEBS Lett.* 556:260–264.
60. Parasassi, T., M. Loiero, …, E. Gratton. 1993. Absence of lipid gel-phase domains in seven mammalian cell lines and in four primary cell types. *Biochim. Biophys. Acta.* 1153:143–154.
61. Van Meer, G., D. R. Voelker, and G. W. Feigenson. 2008. Membrane lipids: where they are and how they behave. *Nat. Rev. Mol. Cell Biol.* 9:112–124.
62. Wang, H. Y., D. Bharti, and I. Levental. 2020. Membrane heterogeneity beyond the plasma membrane. *Front. Cell Dev. Biol.* 8:580814.
63. Levental, I., K. R. Levental, and F. A. Heberle. 2020. Lipid rafts: controversies resolved, mysteries remain. *Trends Cell Biol.* 30:341–353.
64. St Clair, J. W., S. Kakuda, …, E. London. 2020. Induction of ordered lipid raft domain formation by loss of lipid asymmetry. *Biophys. J.* 119:483–492.
65. De Almeida, R. F. M., A. Fedorov, and M. Prieto. 2003. Sphingomyelin/phosphatidylcholine/cholesterol phase diagram: boundaries and composition of lipid rafts. *Biophys. J.* 85:2406–2416.
66. Khmelinskaia, A., J. M. T. Marquês, …, R. F. M. de Almeida. 2020. Liquid-ordered phase formation by mammalian and yeast sterols: a common feature with organizational differences. *Front. Cell Dev. Biol.* 8:337.
67. Kim, H. M., H. J. Choo, …, B. R. Cho. 2007. A two-photon fluorescent probe for lipid raft imaging: C-laurdan. *Chembiochem.* 8:553–559.
68. Klymchenko, A. S. 2017. Solvatochromic and fluorogenic dyes as environment-sensitive probes: design and biological applications. *Acc. Chem. Res.* 50:366–375.
69. Colbasevici, A., N. Voskoboynikova, …, H. J. Steinhoff. 2020. Lipid dynamics in nanoparticles formed by maleic acid-containing copolymers: EPR spectroscopy and molecular dynamics simulations. *Biochim. Biophys. Acta Biomembr.* 1862:183207.
70. Stepien, P., B. Augustyn, …, T. Rog. 2020. Complexity of seemingly simple lipid nanodiscs. *Biochim. Biophys. Acta Biomembr.* 1862:183420.
71. Dupuy, A. D., and D. M. Engelman. 2008. Protein area occupancy at the center of the red blood cell membrane. *Proc. Natl. Acad. Sci. USA.* 105:2848–2852.
72. Overduin, M., C. Trieber, …, J. G. Sheff. 2021. Structures and dynamics of native-state transmembrane protein targets and bound lipids. *Membranes.* 11:451.
73. Kumar, P., G. D. Cymes, and C. Grosman. 2021. Structure and function at the lipid-protein interface of a pentameric ligand-gated ion channel. *Proc. Natl. Acad. Sci. USA.* 118:e2100164118.
74. Dilworth, M. V., H. E. Findlay, and P. J. Booth. 2021. Detergent-free purification and reconstitution of functional human serotonin transporter (SERT) using diisobutylene maleic acid (DIBMA) copolymer. *Biochim. Biophys. Acta Biomembr.* 1863:183602.
75. Brown, C. J., C. Trieber, and M. Overduin. 2021. Structural biology of endogenous membrane protein assemblies in native nanodiscs. *Curr. Opin. Struct. Biol.* 69:70–77.
76. Oot, R. A., Y. Yao, …, S. Wilkens. 2021. Purification of active human vacuolar H+-ATPase in native lipid-containing nanodiscs. *J. Biol. Chem.* 297:100964.
77. Sander, C. L., A. E. Sears, …, K. Palczewski. 2021. Nano-scale resolution of native retinal rod disk membranes reveals differences in lipid composition. *J. Cell Biol.* 220:e202101063.
79. Bernhard, M., and B. Laube. 2020. Thermophoretic analysis of ligand-specific conformational states of the inhibitory glycine receptor embedded in copolymer nanodiscs. *Sci. Rep.* 10, 16569.
79. Jamshad, M., J. Charlton, …, M. Wheatley. 2015. G-protein coupled receptor solubilization and purification for biophysical analysis and functional studies, in the total absence of detergent. *Biosci. Rep.* 35:e00188.
80. Szundi, I., S. G. Pitch, …, D. S. Kliger. 2021. Styrene-maleic acid copolymer effects on the function of the GPCR rhodopsin in lipid nanoparticles. *Biophys. J.* 120:4337–4348.
81. Lorent, J. H., K. R. Levental, …, I. Levental. 2020. Plasma membranes are asymmetric in lipid unsaturation, packing and protein shape. *Nat. Chem. Biol.* 16:644–652.
82. Danielczak, B., and S. Keller. 2020. Lipid exchange among polymer-encapsulated nanodiscs by time-resolved Förster resonance energy transfer. *Methods.* 180:27–34.
83. Cuevas Arenas, R., B. Danielczak, …, S. Keller. 2017. Fast collisional lipid transfer among polymer-bounded nanodiscs. *Sci. Rep.* 7:45875–45878.